

CAUSAL DISCOVERY OF A RIVER NETWORK FROM ITS EXTREMES

BY NGOC M. TRAN

University of Texas at Austin

AND

BY JOHANNES BUCK AND CLAUDIA KLÜPPELBERG

Technical University of Munich

Causal inference for extremes aims to discover cause and effect relations between large observed values of random variables. Over the last years, a number of methods have been proposed for solving the Hidden River Problem, with the Danube data set as benchmark. In this paper, we provide **QTree**, a new and simple algorithm to solve the Hidden River Problem that outperforms existing methods. **QTree** returns a directed graph and achieves almost perfect recovery on the Danube as well as on new data from the Lower Colorado River. It can handle missing data, has an automated parameter tuning procedure, and runs in time $O(n|V|^2)$, where n is the number of observations and $|V|$ the number of nodes in the graph. **QTree** relies on qualitative aspects of the max-linear Bayesian network model.

1. Introduction. Causal inference for extremes has only be considered during the past few years. That observations of climate extremes such as floods, hurricanes, and droughts, but also man-made catastrophes like industry fire, terrorist attacks, or crashes of financial markets have been in the focus of research is convincingly documented in the journal *Extremes*. On the other hand, it is a fundamental problem to assess causality of risks. Often rare events are interconnected; for example, floods disseminate through a river network, and credit markets might fail due to some endogenous systemic risk propagation. Hence, it is necessary to not only understand dependencies between rare events, but also their causal structure.

A benchmark causal inference problem for extremes is the Hidden River Problem [11, 17, 29]. The goal is to recover a river network from *only extreme flows* from a set of $|V|$ stations, *without* any information on the stations or terrain. Here, the true river network serves as the ‘gold standard’, allowing one to verify the performance of the proposed estimator. Beyond extreme value theory, solutions to the Hidden River Problem would directly lead to a new method for the *contaminant tracing* challenge in hydrology [33, 34, 23, 28, 31, 36]. There, one needs an inexpensive method to trace pollutants or chemical constituents transported by an unknown underground waterway. This is highly challenging for existing methods built on fluid mechanics and surveying [2], for contaminants are transported by a complex network of leaky sewage pipes and aquifers that are virtually impossible to measure and model in detail at large scale. Recent advances point towards an imminent data explosion [4, 27], where pollutants exceeding certain thresholds can be detected via a sensor network. Thus, contaminant tracing

MSC 2020 subject classifications: Primary: 05C20, 14T10, 62G32, 62H22 Secondary: 05C99, 62R01, 65S05

Keywords and phrases: Bayesian network, causal model, directed acyclic graph, extreme value statistics, graphical model, machine learning, max-linear model, network, river network, structural equation model, tropical geometry

with sensors data is precisely a version of the Hidden River Problem, where the network is truly unknown.

Over the last years, several methods have been proposed for causal discovery in extremes [11, 15, 16, 17, 18, 19, 20, 21, 29]. A number of these have been applied to solve the Hidden River Problem with the Danube River as the benchmark data set [3], which consists of daily river flow maxima at 31 stations along the Danube. Specifically, the method proposed in [11] returns a highly accurate but undirected graph. [17] correctly estimated a causal order (topological order) on a subset of 12 out of 31 nodes of the Danube using causal tail coefficients. In a recent paper, [29] proposed a method to unveil causal links by assigning expected quantile scores to bivariate data exceeding a sufficiently high threshold in both margins, and causal-induced asymmetries are explored through the minimum description length principle using Kolmogorov’s complexity theory. The approach works well in detecting stream-connected nodes, but often misses or wrongly estimates causal relations, see Table 4.3.

In this work, we give `QTree`, a new and simple algorithm to solve the Hidden River Problem under the assumption that the river network is a root-directed tree. Our method returns a directed graph and has a bootstrap-style automated parameter tuning procedure (cf. Section 2.3). Fitted to 75% randomly chosen subsets of the data, `QTree` achieves almost perfect recovery on the Danube, outperforming existing methods in the literature (cf. Table 4.3, Figure 6).

We further test our method on three sections of the Lower Colorado [26], which are much more challenging data sets. Unlike the Danube, all three sections of the Lower Colorado suffer from severe drought and extreme flooding (cf. Section 3.1.2). In addition, sensors failure on the Lower Colorado create a data set with up to 36.9% of missing data, while the Danube has none. These challenges make recovering the Lower Colorado much closer to the trace contaminant challenge as compared to recovering the Danube. On all three sections of the Lower Colorado, `QTree` fitted to 75% subsets also achieves almost perfect recovery (cf. Section 4).

At a high level, `QTree` aims to fit a *max-linear Bayesian tree* to the data. Max-linear Bayesian networks have recently emerged as a suitable directed graphical model for extremes [1, 13, 14], however, existing methods for learning them aim to learn the model parameters and thus are highly sensitive to model misspecifications [13, 16, 22]. In particular, they have not performed well on the Danube data set. In contrast, `QTree` relies on *qualitative* aspects of the max-linear Bayesian network model to score each potential edge independently, and then applies the Chu-Liu-Edmond algorithm to return the best root-directed spanning tree [12]. We detail the algorithm and the intuition behind it in Section 2. In a forth-coming paper [8], we prove that the tree output by `QTree` is consistent under typical assumptions in extreme value theory.

`QTree` is very flexible, has only two tuning parameters, and is very efficient. It runs in time $O(n|V|^2)$, where n is the number of observations and $|V|$ is the number of nodes. Furthermore, `QTree` maximizes information available from missing data, since at each step it only utilizes the data projected onto two coordinates. For this reason, we believe that `QTree` would be highly suitable for solving the actual trace contaminant challenge with sensors data coming from numerous sensors with potentially a high rate of failure for each sensor. A documented Python implementation of `QTree` is available at [32], along with all data and codes necessary to produce the results and figures in this paper.

Our paper is organized as follows. We introduce `QTree` (cf. Algorithm 1) and `QTree` with automated parameter selection (cf. Algorithm 2) in Section 2. In Section 3, we introduce the data sets, discuss their specific challenges and describe the data preprocessing steps. In

Sections 4 and 5, we give the estimation results of QTree and analyze the performance of the automated parameter selection. Section 6 concludes with a summary.

1.1. *Acknowledgements.* This work is partially supported by a scholarship of the Hanns-Seidel Foundation. We thank the Bavarian Environmental Agency and the Lower Colorado River Authority for providing the original data sets to us. Moreover, we would also like to show our gratitude to the authors of [3] for providing the picture of the upper Danube Basin as well as the declustered data set of the Danube. Ngoc Tran would like to thank the Hausdorff Center for Mathematics and the University of Boon, Germany for making her research visits to Germany possible, which have helped in sparking this collaboration.

1.2. *Notations and basic definitions.* For a set V , let $|V|$ denote its cardinality. A *directed graph* is a pair $G = (V, E)$ of a *node set* V and *edge set* $E = \{j \rightarrow i : i, j \in V, i \neq j\}$. For an edge $j \rightarrow i$, j is called the *parent* and i the *child*. We identify a directed graph G with its adjacency vector $G \in \{0, 1\}^{|V| \times (|V|-1)}$, where $G_{ij} = 1$ iff $j \rightarrow i \in G$. The Hamming distance between two directed graphs G, G' , denoted $d_H(G, G')$ is the Hamming distance between their adjacency vectors, that is, $d_H(G, G') = \sum_{i,j \in V, i \neq j} \mathbf{1}_{\{G_{ij} \neq G'_{ij}\}}$. A directed acyclic graph (abbreviated DAG) is a directed graph with no directed cycles. Say that i is reachable from j , denoted $j \rightsquigarrow i$, if there exists a directed path from j to i . For a DAG G , its reachability graph G^* is defined as $G^*_{ij} = 1$ iff $j \rightsquigarrow i, j \neq i$. For a sample \mathcal{X}' of n points in \mathbb{R} , write $Q_{\mathcal{X}'}(p)$ for its p -th quantile, $p \in (0, 1)$.

2. The algorithm.

2.1. *Motivations from the max-linear Bayesian networks.* A max-linear Bayesian network [14] is defined by the recursive structural equation

$$X_i = \bigvee_{j:j \rightarrow i \in \mathcal{D}} c_{ij} X_j \vee Z_i, \quad c_{ij}, Z_i \geq 0, i \in V, \quad \mathcal{D} \text{ a DAG on } V. \quad (2.1)$$

Here $C = (c_{ij} \geq 0)$ is a fixed $V \times V$ matrix of coefficients supported on a directed acyclic graph (DAG) \mathcal{D} on node set V , and $Z \in \mathbb{R}_{\geq 0}^V$ is a random vector of unknown *sources* (innovations). Applied to a river network, \mathcal{D} represents the river network, X_i an extreme discharge at node i , Z_i is ‘nature’s input’ (eg: rainfall) at station i , and c_{ij} is some measure of flow rate from station j to station i . The model says that this extreme discharge is either the result of an external input Z_i , or that it is the weighted maximum of discharges from the parent nodes of i in \mathcal{D} .

Max-linear Bayesian networks have foundations in extreme value theory and have been investigated in [1, 13, 14, 16]. Noisy versions of the model have been considered in [7]. Existing statistical learning methods have focused on estimating the reachability matrix C^* of C , as this is the identifiable component of the model [13, 16]. These methods include the generalized MLE [13, 16], the tail dependence estimator [15], and the scaling estimator [21]. In [21], a two-step new structure learning and estimation algorithm for the recursive max-linear model from (2.1) has been developed, which first estimates a causal order and then the dependence parameters of the model. All of these methods work well for noise-free data, that is, samples obtained directly from (2.1) or (2.2). However, they do not perform well under noise or on data set such as the Danube or the Lower Colorado.

For numerical stability, in practice, one often considers the point-wise logarithm of extreme measurements. From now on we assume that the data has been log-transformed. To avoid introducing new symbols, we keep the same notation, so the max-linear Bayesian network becomes

$$X_i = \bigvee_{j:j \rightarrow i \in \mathcal{D}} (c_{ij} + X_j) \vee Z_i, \quad c_{ij} \in \mathbb{R} \cup \{-\infty\}, Z_i \in \mathbb{R}, i \in V, \quad \mathcal{D} \text{ a DAG on } V. \quad (2.2)$$

In this paper, we see the Hidden River Problem as the problem of learning the support of max-linear Bayesian networks over *root-directed trees*.

Problem 1 (Hidden River Problem under the max-linear Bayesian tree model). Assume that (c_{ij}) is supported on a root-directed spanning tree \mathcal{T} on V . That is, each node i in \mathcal{T} has *exactly one child*, except the (unknown) root, which has no children. Given n observations $\mathcal{X} = \{x^1, \dots, x^n\}$ generated via (2.2) and corrupted with noise, find \mathcal{T} .

The root-directed tree assumption is reasonable for a river where the measurement nodes are placed sufficiently far apart, such as the Danube. Importantly, this assumption allows the tree \mathcal{T} to be uniquely identified by its reachability graph \mathcal{T}^* , and thus is identifiable [13]. In contrast, for general max-linear Bayesian networks, only \mathcal{T}^* is identifiable.

LEMMA 2.1. *If \mathcal{T} is a root-directed tree, then its reachability graph \mathcal{T}^* uniquely defines \mathcal{T} .*

PROOF. Since \mathcal{T} is a tree, any directed path between two nodes in \mathcal{T} is unique. Thus, \mathcal{T}^* has the property that $i_0 \rightarrow i_1 \rightarrow \dots \rightarrow i_k \subset \mathcal{T}^*$ if and only if $i_r \rightarrow i_{r'} \in \mathcal{T}^*$ for all $0 \leq r < r' \leq k$. Therefore, for $i \in V$, $j \rightarrow i \in \mathcal{T}$ if and only if $j \rightarrow i \in \mathcal{T}^*$ and that there is no descendant k of j in \mathcal{T}^* such that $k \rightarrow i \in \mathcal{T}^*$. This means \mathcal{T} is uniquely recoverable from \mathcal{T}^* . \square

We stress that the root-directed tree assumption is *different* from the usual tree in Bayesian networks, where each *child* has at most one parent. Learning the single-parent tree can be done with the message passing algorithm, which recursively identifies the parent of a node through likelihood calculations [35]. This strategy does not work for the root-directed tree, since each child can have multiple parents.

In general, learning Bayesian networks with more than one parent is NP-hard [9]. However, it follows from [14, Theorem 2.2] that learning the max-linear Bayesian networks from i.i.d *noise-free samples* is solvable in time $O(|V|^2n)$ with $O(|V|(\log(|V|))^2)$ samples.

LEMMA 2.2. *Let $\mathcal{X} = \{x^1, \dots, x^n\}$ be i.i.d exact samples from (2.2), not corrupted with further noise. Assume that the Z_i 's are independent and have continuous distributions. Define*

$$\hat{c}_{ij} = \min_{x \in \mathcal{X}} (x_i - x_j). \quad (2.3)$$

Suppose that for each edge $j \rightarrow i$ such that $c_{ij} > -\infty$, there exist at least two observations $x \in \mathcal{X}$ where j causes i . Then C^ can be uniquely recovered from \hat{C} since*

$$\hat{c}_{ij} = c_{ij}^* \iff \text{min in (2.3) is achieved at least twice.} \quad (2.4)$$

In particular, c^* can be computed in time $O(|V|^2n)$. If one assumes that at each node, the parents are independently and equally likely to be the one that achieves the maximum, then for $n = O(|V|(\log(|V|))^2)$ observations, one has a high probability of recovering C^* exactly.

PROOF. Note that $x_i \geq c_{ij}^* + x_j$ for all $x \in \mathcal{X}$, and if $j \rightarrow i$ in observation x , then $x_i = c_{ij}^* + x_j$. Rearrange, we get (2.3). Equation (2.4) is [14, Theorem 2.2]. Now we prove the complexity claim. Since there are $O(|V|^2)$ many edges, and for each edge we need $O(n)$ operations to compute the minimum in (2.3), the complexity is $O(|V|^2n)$. The number of observations needed is so that each edge is seen at least twice is a variant of coupon-collecting [5, 6], where each node must collect two coupons (parents) among its set of parents. Since the nodes are collecting the coupons simultaneously, by the union bound, the number of observations needed is at most $\log(|V|)$ times the number of observations needed for the node with highest degree to collect all of its coupons, which in turn is $O(|V| \log(|V|))$. \square

The estimator in (2.3) relies on a value to be observed exactly at least twice, and is thus very sensitive to noise. Unsurprisingly, it does not perform well as-is on real data, or even simulations of the max-linear model with independent noise. However, there are two interesting qualitative implications of Lemma 2.2. First, to tell spurious edges from real ones, (2.4) says that the empirical distribution of

$$\{x_i - x_j : x \in \mathcal{X}\} \quad (2.5)$$

is concentrated *at* the minimum of its support if and only if $j \rightarrow i$. Thus, if the noise is small, one can expect to see a concentration *near* the minimum of $x_i - x_j$ when $j \rightarrow i \in \mathcal{D}$. Second, Lemma 2.2 says that only *two* ‘high-quality’ observations are enough to identify an edge $j \rightarrow i$. In other words, one may want to replace $\{x_i - x_j : x \in \mathcal{X}\}$ by a different set computable from \mathcal{X} whose distribution is even *more* concentrated near its minimum, and thus would be more robust to noise. By (2.2), $x_i \geq \max_{j'}(c_{ij'} + x_{j'})$, so $x_i = c_{ij} + x_j$ at some observation $x \in \mathcal{X}$ implies $x_j > (c_{ij'} - c_{ij}) + x_{j'}$ for all $j' \neq j$. In other words, if $j \rightarrow i \in \mathcal{T}$, then it is more likely to find these ‘high-quality’ observations conditioned on the event that x_j is large. A natural candidate for ‘large’ is to lie above $Q_{\mathcal{X}_j}(q)$, the q -th quantile of the empirical distribution of \mathcal{X} in the j -th coordinate. That is, one would want to replace (2.5) by the set

$$\mathcal{X}_{ij}(q) := \{x_i - x_j : x \in \mathcal{X}, x_j > Q_{\mathcal{X}_j}(q)\}. \quad (2.6)$$

These two observations, concentration near the lower tails of $x_i - x_j$ and conditioning on large marginal values of x_j , are the motivations behind QTree.

2.2. The algorithm. Algorithm 1 computes independently for each potential edge $j \rightarrow i$ a score d_{ij} , seen as a measure of dispersion of $\mathcal{X}_{ij}(q)$ near its minimum, then outputs the minimum directed spanning tree of the weighted graph $D = (d_{ij})$. The idea is that the true edge $j \rightarrow \text{ch}(j)$ would have the lowest dispersion (highest concentration) among all potential outgoing edges at each node j . In an upcoming work [8], we confirm this statement under the assumption that the data truly come from a noise-corrupted max-linear Bayesian network with distributional assumptions typical to extreme value theory.

There are several possible choices for a dispersion measure. For example, one could fix a pair of quantiles $0 < \underline{r} < \bar{r} < 1$, and consider the quantile gap

$$d_{ij}(\underline{r}, \bar{r}) := \left(\frac{Q_{\mathcal{X}_{ij}(q)}(\underline{r}) - Q_{\mathcal{X}_{ij}(q)}(\bar{r})}{\sqrt{n_{ij}}} \right)^2, \quad (2.7)$$

where $n_{ij} = |\mathcal{X}_{ij}(q)|$ is the number of observations in the set $\mathcal{X}_{ij}(q)$ defined in (2.6). We note that the normalization factor n_{ij} only matters when missing values are unevenly distributed across pairs, such as the case of the Lower Colorado river (cf. Section 3.1.2). Then, pairs with less observations get a relative penalty in the dispersion estimate to account for fluctuations in sample quantile estimates due to small samples. If no missing values are present, as is the case with the Danube, then $n_{ij} = n \cdot q$ for all pairs (i, j) , and the algorithm would return the exact same tree \hat{T} if dispersion was defined without the denominator, that is,

$$d_{ij}(\underline{r}, \bar{r}) = \left(Q_{\mathcal{X}_{ij}(q)}(\underline{r}) - Q_{\mathcal{X}_{ij}(q)}(\bar{r}) \right)^2.$$

If \bar{r} is small, then $d_{ij}(\underline{r}, \bar{r})$ is a local measure of dispersion in the lower tail of $\mathcal{X}_{ij}(q)$. However, this gives two parameters to tune in addition to q , and if the number of observations are small, then \bar{r} cannot be too small. Our intention in this paper is to produce a versatile, nonparametric estimation method that can scale to large data sets, with *minimal* number of tuning parameters. Therefore, for simplicity, we replace the \bar{r} -th quantile in (2.7) by the mean over the set $\mathcal{X}_{ij}(q)$. This leads to the following default dispersion measure for QTree.

$$d_{ij}(\underline{r}) := \left(\frac{Q_{\mathcal{X}_{ij}(q)}(\underline{r}) - \mathbb{E}(\mathcal{X}_{ij}(q))}{\sqrt{n_{ij}}} \right)^2. \quad (2.8)$$

Algorithm 1 QTree

Parameters: $\underline{r} \in (0, 1)$, $q \in (0, 1)$.

Input: samples $\mathcal{X} \in \mathbb{R}_{\geq 0}^{n \times d}$.

Output: a root-directed spanning tree \hat{T} on V .

- 1: **for** $j \rightarrow i$, $j, i \in V$, $j \neq i$ **do**
 - 2: Compute $d_{ij}(\underline{r})$ by (2.8).
 - 3: Compute $\hat{T} :=$ minimum directed spanning tree on the directed graph $D = (d_{ij}(\underline{r})) \in \mathbb{R}^{d \times d}$ with the Chu-Liu-Edmond algorithm[10],
 - 4: **return** \hat{T}
-

We note that the complexity of computing QTree is the same as that of computing the simple estimator (2.3), which is $O(|V|^2 n)$.

LEMMA 2.3 (Complexity of QTree). *Algorithm 1 runs in time $O(|V|^2 n)$.*

PROOF. For each pair $i, j \in V$, $i \neq j$, to compute d_{ij} , one needs to compute the q -th quantile of \mathcal{X}_j , the \underline{r} -th quantile and the mean of $\mathcal{X}_{ij}(q)$. Since q and \underline{r} are fixed in advance, the quantiles can be computed in time $O(n)$ [30]. As there are $O(|V|^2)$ pairs, computing $D = (d_{ij})$ takes $O(|V|^2 n)$. The Chu-Liu-Edmond algorithm runs on the complete bidirected graph D , and thus takes $O(|V|^2)$ [12]. So the complexity of QTree is $O(|V|^2 n + |V|^2) = O(|V|^2 n)$. \square

2.3. *Parameter tuning without knowledge of the true graph.* For real trace contaminant applications, the true tree \mathcal{T} is unknown, one needs a way to select the model parameters without knowledge of the true graph. In this section, we propose a cross-validation procedure to automatically choose q and \underline{r} . Algorithm 2 presents the complete QTree algorithm with automated parameter selection.

QTree has two parameters: the quantile $\underline{r} \in (0, 1)$ and the cut-off quantile $q \in (0, 1)$. If the data perfectly came from a truncated max-linear Bayesian tree, then we should select

\underline{r} as small as possible while making q as large as possible to minimize error. However, due to the presence of noise, setting \underline{r} too small would make the estimator volatile to outliers. Similarly, the larger q is, the higher the concentration of $F_{ij}(q)$ at its minimum if the model was correctly specified, but also the less samples we have available to estimate its quantile concentration. Therefore, a good indicator of the model performance is a measure of variability in the estimated tree, that is, whether this tree \hat{T} and its reachability matrix \hat{R} would change significantly if we fit QTree to different data sets. To simulate different data sets, we can randomly sample subsets of the given data. Thus, we need a definition of variability of a distribution of directed spanning trees. Here is the formal definition that we propose.

DEFINITION 2.4. Let $\mathbb{T} = \{T^1, \dots, T^m\}$ be a collection of directed spanning trees on V nodes, and let $\mathbb{R} = \{R^1, \dots, R^m\}$ be their corresponding reachability DAGs. The centroid of \mathbb{T} , denoted $\mathbb{E}(\mathbb{T})$, is the directed spanning tree on V nodes that minimizes the expected Hamming distance to a randomly chosen tree in \mathbb{T} , that is

$$\mathbb{E}(\mathbb{T}) := \arg \min \left\{ \sum_{i=1}^m d_H(T, T^i) : T \text{ a directed spanning tree on } V \right\}. \quad (2.9)$$

Let $\mathbb{E}(\mathbb{R})$ denote the reachability DAG of $\mathbb{E}(\mathbb{T})$. Let e_T be the number of edges of $\mathbb{E}(\mathbb{T})$, and e_R be the number of edges of $\mathbb{E}(\mathbb{R})$, respectively. The variability of \mathbb{T} , denoted $\text{Var}(\mathbb{T})$, is

$$\text{Var}(\mathbb{T}) := \frac{1}{e_T} \frac{1}{m} \sum_{i=1}^m d_H(T^i, \mathbb{E}(\mathbb{T})) + \frac{1}{e_R} \frac{1}{m} \sum_{i=1}^m d_H(R^i, \mathbb{E}(\mathbb{R})). \quad (2.10)$$

The reachability graph in (2.10) penalizes the situation where T^i and $\mathbb{E}(\mathbb{T})$ differ in a few edges low down in the tree, for example, if they have different roots. Such a difference would lead to small Hamming distance between the two trees, but a large Hamming distance between their reachability graphs, and in particular, very different river networks.

The following lemma says that $\mathbb{E}(\mathbb{T})$ is the **maximum** directed spanning tree of a particular graph $W(\mathbb{T})$ that measures the agreement among the trees in \mathbb{T} . In particular, $\mathbb{E}(\mathbb{T})$ can be computed in using the Chu-Liu-Edmond algorithm, and thus $\text{Var}(\mathbb{T})$ can be computed in polynomial time.

LEMMA 2.5. Let $\mathbb{T} = \{T^1, \dots, T^m\}$ be a collection of directed spanning trees on V nodes. Define $W(\mathbb{T}) \in \mathbb{R}_{\geq 0}^{d \times d}$ by

$$W(\mathbb{T})_{ij} := \#\{T \in \mathbb{T} : j \rightarrow i \in T\}. \quad (2.11)$$

Suppose that the maximum directed spanning tree T^* of the graph on V with weight matrix $W(\mathbb{T})$ is unique. Then $\mathbb{E}(\mathbb{T}) = T^*$.

PROOF. Identify a directed tree T with the vector $(T_{uv}) \in \{0, 1\}^{|V|^2 - |V|}$. Write $\mathbf{1} = (\mathbf{1}_{uv})$ for the all-one vector of the same dimension. Let T' be a directed spanning tree on V . Our goal is to show that

$$\sum_{i=1}^m d_H(T', T^i) \geq \sum_{i=1}^m d_H(T^*, T^i),$$

which would establish that $T^* = \mathbb{E}(\mathbb{T})$ by (2.9). Indeed,

$$\begin{aligned}
\sum_{i=1}^m d_H(T', T^i) &= \sum_{i=1}^m \sum_{u,v \in V: u \neq v} \mathbf{1}\{T'_{uv} \neq T^i_{uv}\} = \sum_{u,v \in V: u \neq v} \sum_{i=1}^m \mathbf{1}\{T'_{uv} \neq T^i_{uv}\} \\
&= \sum_{u,v \in V: u \neq v} (W_{uv} \mathbf{1}_{u \rightarrow v \notin T'} + (m - W_{uv}) \mathbf{1}_{u \rightarrow v \in T'}) = \langle W, \mathbf{1} - T' \rangle + \langle m\mathbf{1} - W, T' \rangle \\
&= -2\langle W, T' \rangle + \langle W, \mathbf{1} \rangle + \langle m\mathbf{1}, T' \rangle \\
&= -2\langle W, T' \rangle + \langle W, \mathbf{1} \rangle + m(d-1) \quad \text{since } T' \text{ is a spanning tree on } V \\
&\geq -2\langle W, T^* \rangle + \langle W, \mathbf{1} \rangle + m(d-1) \quad \text{by definition of } \mathbb{E}(\mathbb{T}) \\
&= -2\langle W, T^* \rangle + \langle W, \mathbf{1} \rangle + \langle m\mathbf{1}, T^* \rangle \quad \text{since } T^* \text{ is a spanning tree on } V \\
&= \sum_{i=1}^m d_H(T^*, T^i).
\end{aligned}$$

□

Algorithm 2 QTree with automated parameter selection

Parameters: cross-validation parameters $f \in [0, 1]$ and number of repeats $m \in \mathbb{N}$, a set of parameters $\Theta = \{(\underline{r}, q)\} \subset (0, 1)^2$ to search over.

Input: samples $\mathcal{X} = \{x^1, \dots, x^n\} \subset \mathbb{R}^V$.

Output: the optimal parameter $(\underline{r}^*, q^*) \in \Theta$ and the corresponding directed spanning tree \hat{T} on V .

- 1: **for** $(\underline{r}, q) \in \Theta$ **do**
 - 2: **for** $\ell = 1, \dots, m$ **do**
 - 3: Sample without replacement a random subset \mathcal{X}^ℓ of $n \cdot f$ observations from \mathcal{X}
 - 4: Let T^ℓ be the output of QTree(\underline{r}, q) fitted on \mathcal{X}^ℓ .
 - 5: Let $\mathbb{T}(\underline{r}, q) = \{T^\ell : \ell = 1, \dots, m\}$
 - 6: Compute $W(\mathbb{T}(\underline{r}, q))$ by (2.11)
 - 7: Compute $\mathbb{E}(\mathbb{T}(\underline{r}, q))$ as the maximum directed spanning tree of $W(\mathbb{T}(\underline{r}, q))$ per Lemma 2.5.
 - 8: Compute $\text{Var}(\mathbb{T}(\underline{r}, q))$ by (2.10)
 - 9: Define $(\underline{r}^*, q^*) := \arg \min\{\text{Var}(\mathbb{T}(\underline{r}, q)) : (\underline{r}, q) \in \Theta\}$.
 - 10: **Return** the pair (\underline{r}^*, q^*) and the tree $\mathbb{E}(\mathbb{T}(\underline{r}^*, q^*))$.
-

LEMMA 2.6. *Algorithm 2 has complexity $O(|V|^2 nm |\Theta|)$.*

PROOF. For each pair $(\underline{r}, q) \in \Theta$, step 3 takes $O(mn)$ and step 4 takes $O(|V|^2 nm)$ by Lemma 2.3. Step 6 takes $O(m|V|^2)$, and step 7 takes $O(|V|^2)$ by Chu-Liu-Edmond. Computing the reachability graph for a directed tree on $|V|$ nodes takes $O(|V|)$, so step 8 takes $O(m|V|^2)$, since for each of the m trees $T^\ell \in \mathbb{T}$ we need to compute its Hamming distance from the estimated tree $\mathbb{E}(\mathbb{T})$. So, for each pair $(\underline{r}, q) \in \Theta$, steps 3 to 8 take $O(|V|^2 nm)$ time. Thus overall, the algorithm complexity is $O(|V|^2 nm |\Theta|)$. □

3. Data description.

3.1. *From daily maxima to extreme discharges.* In any river, temporal dependence causes extreme discharges at a given station to occur in clusters [3]. Furthermore, extreme discharges at upstream stations may cause extreme discharges at downstream stations some days later.

As all these extremes should be analysed as being part of the same event, the data must be declustered.

In [3], the authors put forward a declustering method on the Danube to obtain extreme discharge measurements from daily observations. The idea is to find non-overlapping time windows of p days, centered around the observation of maximal rank across all series. For each series, one then takes the maximum within the given time window, deletes the data of this window and proceeds until no window of p consecutive days remains. For details on this procedure, see [3]. In this paper, for the Danube, we use the declustered data provided by [3]. For the Lower Colorado, multiple dams cut off the river into disjoint sections, and many nodes have excessive amounts of missing data. As these problems were not present in the Danube data set, we split the rivers into three sections based on the dam locations, and remove nodes with excessive missing values, or nodes which are within 10km of a major dam and then apply the same declustering procedure to the Colorado as [3]. These sections, called the upper, middle and lower Colorado, respectively, are then treated as three separate networks with three separate data sets. We have taken care to keep as many nodes as possible. The resulting three sub-networks for the entire Lower Colorado can be found in Figure 15. As seen in Table 3.1, missing data affect all three subrivers, especially the lower section. Section 3.1.2 below details the data processing steps on the Lower Colorado.

	lower Colorado	middle Colorado	upper Colorado
average missing data	36.9%	27%	18.4%

TABLE 3.1

Average missing data for each of the three sections of the Lower Colorado in the final data set, consisting of declustered extreme discharges taken over $p = 8.5$ days windows.

3.1.1. *The Upper Danube Basin.* The declustered Danube data set provided by [3] consists of extreme river discharges measured at 31 stations, see Figure 1. The data is based on 50 years of daily mean river discharges from 1960–2009 in m^3/s and has been originally made available by the Bavarian Environmental Agency (<http://www.gkd.bayern.de>). To account for seasonality, [3] only consider the summer months June, July and August which leads to $n = 428$ events at all of the 31 gauging stations, with no missing data. Discussions on hydrological and anthropogenic models, the influence of flood impact variables and the flood risk management system in Germany concerning these data can be found in [3, 29].

3.1.2. *The Lower Colorado Basin.* The Colorado (Texas) is one of the major rivers in Texas. We consider the Lower Colorado Basin which has caught particular interest by authorities as floodings in this area occur regularly and are especially devastating. The basin is managed by the Lower Colorado River Authority (LCRA). They collect data on both, river discharges and rainfall in the Lower Colorado River Basin in Texas. We are using river discharge data from the 1st of December 1991 to the 14th of April 2020 which is measured in cubic feet per second (cfs) and has been provided by the LCRA (<https://www.lcra.org/>).

The climate of Texas is marked by little precipitation resulting in drained small rivers and creeks most of the times (that is, a discharge of 0). However, during heavy storm events, drained creeks regularly develop an excess peak water flow, flooding the surrounding area. To reduce the risk of flood, there are several dams located in the Lower Colorado Basin, see Figure 15. This effectively creates a partition of the river into disjoint sections. Moreover, during storm events, sensors that measure river discharges can get damaged, resulting in loss

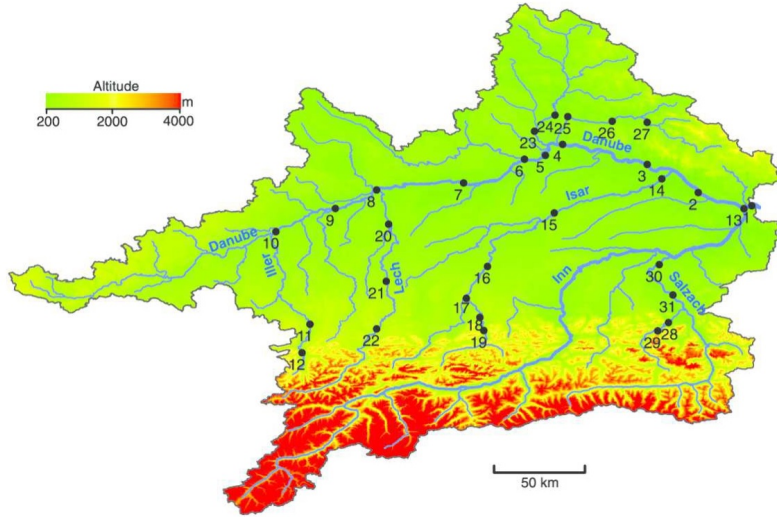


Fig 1: The Upper Danube Basin

of data, see Figure 2. Since we need to account for all these difficulties, the data set of the Colorado is much more challenging compared with the Danube.

The raw data provided by LCRA contains a total of 104 nodes located around the Colorado river and its tributaries. We omit four nodes of the Blanco River and one node of the San Bernard River, since neither are stream-connected to the Colorado River. Moreover, we exclude the nodes 5476, 5634, 5635, 6397 and 6533 as they are located close to hydropower plants. This gives us a total of 94 nodes. Twenty-one of these nodes have no data, and thus are excluded, leaving 73 nodes. The resulting tree induced by water flow connections can be found in Figure 15. The median discharges at the 73 nodes range from 0 to almost 1600 cfs. However, even mostly drained rivers still develop a significant peak water discharge. For example, Figure 2 shows a typical discharge at various nodes around one storm event. Node 3 has a median discharge of only 15 cfs and is hence mostly drained, the water flow regularly aggregates to over 16,000 cfs within a very short period of time. These extreme discharges occur during heavy storm events that are typical for the climate of Texas, which can turn drained creeks into medium to large sized rivers for some small period of time, causing flooding damages to surrounding areas.

Sensors usually measure the river discharge several times per hour. Since storm events and the associated river discharges can last as little as 12 hours, we divide each day into two intervals of 12 hours each. We then take the maximum for each sensor over each 12 hour period. The number of 12 hour observation windows then ranges from only 55 to 20673. After this step, we omit node 2640, as the physical distance between nodes 10 and 2640 is only 2000 feet and node 10 contains more than 50% of additional daily observations.

Within the river network, there are several dams that have different purposes ranging from water supply to hydroelectric power and flood management, see [25]. Since these dams partition the river into effectively disjoint sections, and since QTree assumes that there is one spanning tree for all nodes, it is necessary for us to split the Lower Colorado into sub-rivers based on the dams locations. We therefore look for the biggest possible subset of nodes such that (i) there is no large dam in between and (ii) there are at least 10 kilometers between

a dam and an up- or downstream node as the crow flies. For tributaries, there are at least 10 kilometers between a dam and its river mouth. This leads to two subsets of the Lower Colorado Basin, an upper part and a lower part. Additionally, we also consider a network of tributaries of the Colorado around the middle of the Lower Colorado Basin. While this subset is separated by the Llano River Dam, an analysis has shown that the dam is too small to interfere with the estimation results. We refer to this as the middle Colorado, while the two previously mentioned subsets as the upper and lower Colorado, respectively.

Up to this step, we obtain three data sets: the upper, middle and lower parts of the Lower Colorado, with 9, 12 and 25 nodes, respectively. From here on we treat these three sections as three separated, unrelated sub-rivers. The three data sets combined have 33.8% of missing data. Across all three data sets, there is not a single observation having no missing data at all nodes.

For each sub-river of lower, middle and upper Colorado, we keep the biggest subset of nodes such that for any pair (j, i) of this subset, there are at least 1000 pair-wise daily observations. This ensures that among the given pair of nodes, any possible causal relations can be discovered, and not be affected by the lack of concurrent data. This omits nodes 45, 5422, 6386 and 6475, all of which lie by the lower Colorado. The final three data sets for the entire Lower Colorado can be found in Figure 15.

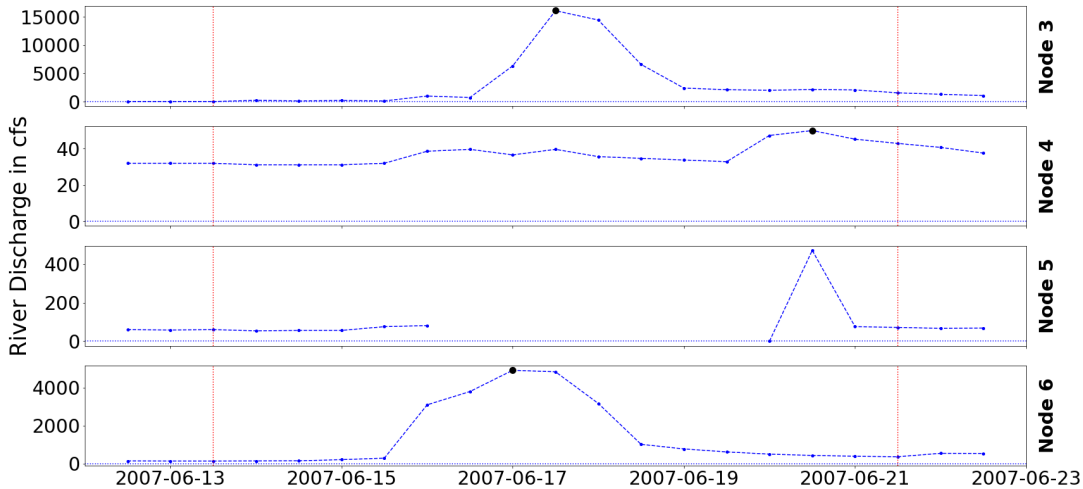


Fig 2: Declustering with missing data on the Lower Colorado. The red lines mark a time window of $p = 8.5$ days. In node 3,4 and 6, a black dot denotes the peak discharge during this window. In node 5, the sensor did not function during this entire time period, so the peak for node 5 is marked as a missing value.

For each of the three data sets, we now apply the declustering approach of [3], where we choose $p = 8.5$ days, corresponding to 17 half-days. We note that during storm events that usually result in huge river discharges, sensors can break before the river reaches peak discharge. For practical reasons, the sensors only get replaced when the storm event is over [24] (Figure 2). This means that the sensor potentially did not measure the largest possible water discharge that occurred at a given node i . Therefore, during the declustering step, for a fixed node i , we check if there is any missing data within the time window we consider. If there is, we do not assign any value for node i for the given window (assume missing). This

can be seen in Figure 2, where we do not assign any value for node 5 due to missing data in the given time window.

3.1.3. Properties of the final upper, middle and lower Colorado data sets. The final three data sets, available at [32], are the results of the preprocessing procedure described the previous section. The upper Colorado data set contains 9 nodes, ranging between the O.H. Ivie Reservoir to Lake Buchanan, including the Colorado river, Pecan Bayou as well as the San Saba River and Brady Creek (cf. Figure 3). Figure 4 depicts the middle Colorado along with the 12 nodes in the final data set. These nodes sit on different rivers and creeks, the most prominent being the Llano river.

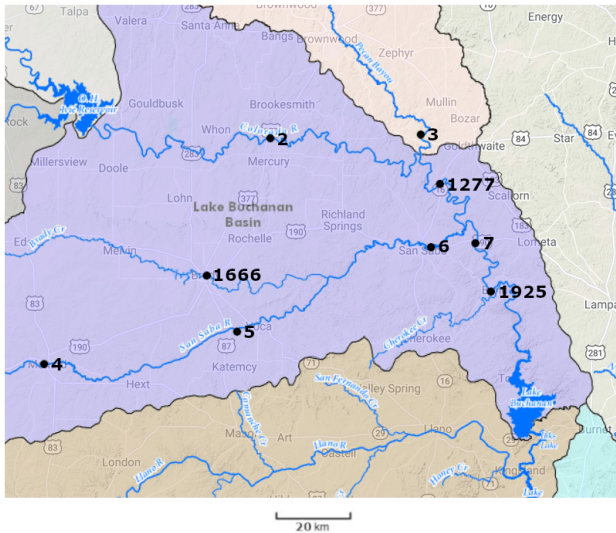


Fig 3: The upper Colorado

The lower Colorado is the largest part we consider. Starting south of Austin, the final data set contains 21 nodes over a distance of more than 150 miles (Figure 5). From these 21 observations, ten are located along the Colorado river (5423, 5450, 21, 5525, 42, 22, 23, 6377, 24, 6537) and the rest are located along tributaries. Due to the flood management, we can see a strong concentration of measurement points around the city of Austin, with some points lying only few miles apart from each other. The close proximity of these nodes induce a strong spatial dependence even among nodes which are not stream-connected, making it potentially more challenging to recover the true network.

4. Results. For each of the four river networks (Danube, upper, middle and lower section of the Lower Colorado), we fitted **QTree** with fixed $\underline{r} = 0.05$, and q chosen automatically from $\{0.7, 0.75, 0.8, 0.85, 0.9, 0.95\}$ using Algorithm 2, with subsampling rate $f = 0.75$ and number of repetitions $m = 1000$. The main reason we fixed \underline{r} and varied q is for ease of visualization, as the performance of the automatic tuning procedure can be visualized with a two-dimensional plot (cf. Section 5). The parameters q selected by **QTree** for these rivers are shown in Table 4.2.

Figures 6 to 8b show the estimated trees of the Danube, upper, middle and lower sections of the Lower Colorado, respectively. Blue edges are correct. Gray edges are missing (in the true network but not in the estimated). For incorrectly estimated edges, we color them differently depending on whether they are stream-connected. If they are, we color them brown to indicate

	Danube	Lower Colorado	Lower Colorado (150)	Middle Colorado	Upper Colorado
q	0.775	0.85	0.725	0.75	0.825

TABLE 4.2

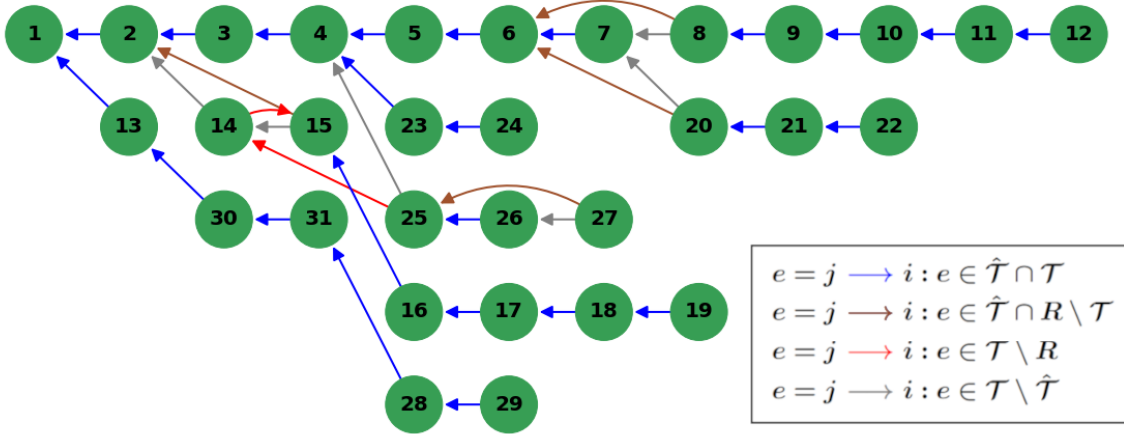
Parameters q selected by QTree.

Fig 6: Estimated Danube network. Blue edges are correct edges, brown edges are wrong in graph but correct in reachability, red edges are wrong in graph and reachability, gray edges are missing edges.

Similarly, QTree almost perfectly recovers the upper and middle Colorado, which are relatively small networks. For the upper Colorado (Figure 7, left), with a total of 9 nodes, the method returns only one wrong edge from $2 \rightarrow 7$, skipping node 1277. For the middle Colorado (Figure 7, right), we again have one wrong edge ($2625 \rightarrow 8$). Despite the mistake being more severe in the middle Colorado as these two nodes are not stream-connected, one can conclude that QTree gives very good results on small river networks even in the presence of missing data.

Finally, in Figure 8a, we visualize the estimation of the lower Colorado. This data set is the most challenging, as the amount of missing data is much more severe, see Table 3.1. In particular, the nodes 5525, 5450, 5423, 5435 and 5524 suffer from very few observations (less than 150 observations each). Additionally, as previously mentioned, nodes are spatially clustered around the city of Austin. Nevertheless, even for this data set QTree has only two red edges between 6537 and 24 and between 42 and 5525. These pair of nodes, however, are directly connected by an edge, and from Figure 5, we can see that they both lie very close to each other such that the mistake can be considered as less serious. All the remaining wrong edges are stream-connected and usually only skip one or two nodes with the exception of the edge $5435 \rightarrow 23$. We note that the majority of the errors made by QTree involve the nodes with less than 150 observations. This is not at all surprising. The model was fitted to only 75% of the data, and the optimally chosen q is 0.85, which means that for each edge involving one of the above nodes, the number of observations available to QTree is at most $150 \times 0.75 \times 0.15 = 14$. To check the hypothesis that this threshold is too small for QTree to perform reliably, we excluded all nodes with less than 150 observations. This reduces the set of nodes to 16, erasing the previously mentioned 5 nodes. We then again use QTree with automated parameter selection. The result can be found in Figure 8b. The estimation has

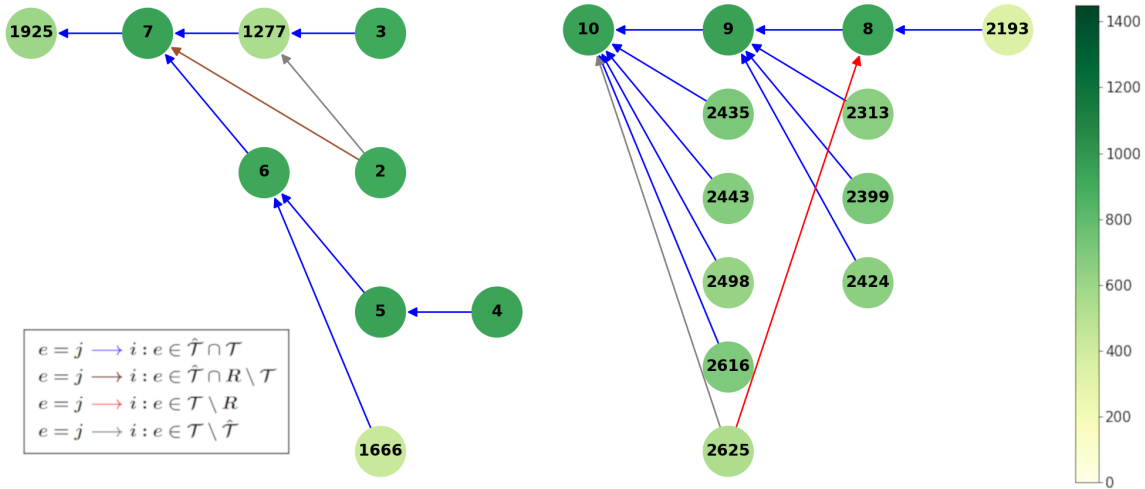


Fig 7: Estimated upper (left) and middle Colorado (right). Node colors represent the amount of available data after declustering.

greatly improved. The amount of red edges decreased by one while the amount of brown edges is reduced to one edge only skipping a single node. This shows another desirable feature of QTree, namely, that it relies on local (pairwise) estimation, and thus changes to the node set in one part of the tree does not affect the estimated network elsewhere.

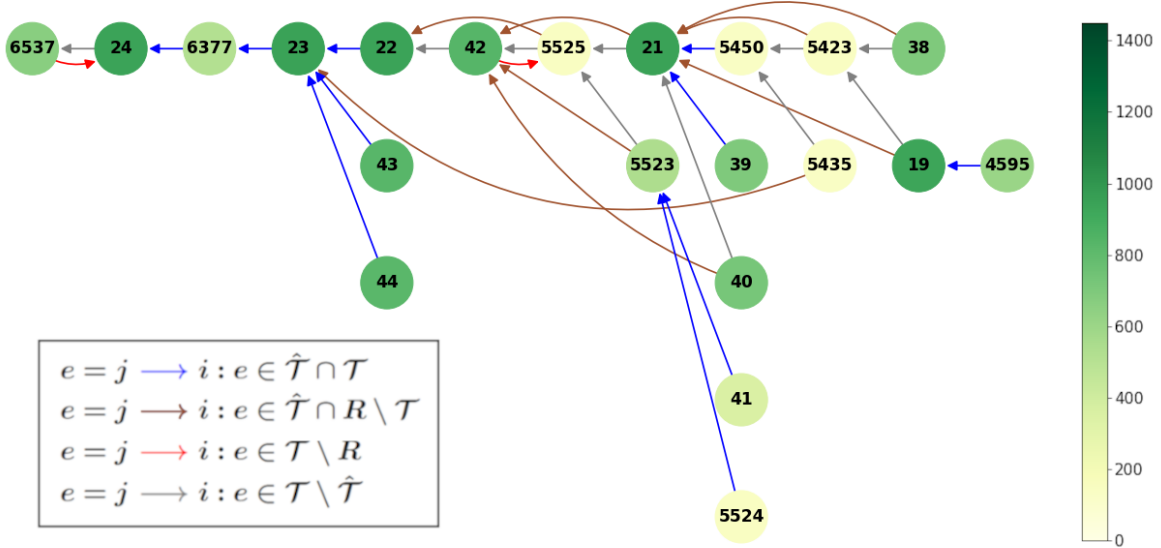
In conclusion, our algorithm has been proven to work reliably on all of the four data sets considered. For the Danube, despite the large number of nodes, we only have six wrongly set edges with four of them just skipping a single node. For the Colorado, despite the significant fraction of missing data (cf. Table 3.1), large fluctuations between base flow and extreme flow, and the close spatial proximity between nodes, we still achieve very good results.

4.1. *Performance metrics.* Table 4.3 summarizes the results of QTree on the four networks using the following standard metrics from causal inference [37]: normalized Structural Hamming Distance (nSHD), True Positive Rate (TPR), False Discovery Rate (FDR) and False Positive Rate (FPR). We recall their definitions below. Let G be the true graph and \hat{G} be the estimated graph. Define the structural Hamming distance $\text{SHD}(G, \hat{G})$ between G and \hat{G} as the minimum number of edge additions, deletions and reversals to obtain G from \hat{G} . The normalized structural Hamming distance $\text{nSHD}(\hat{G}, G)$ is defined as

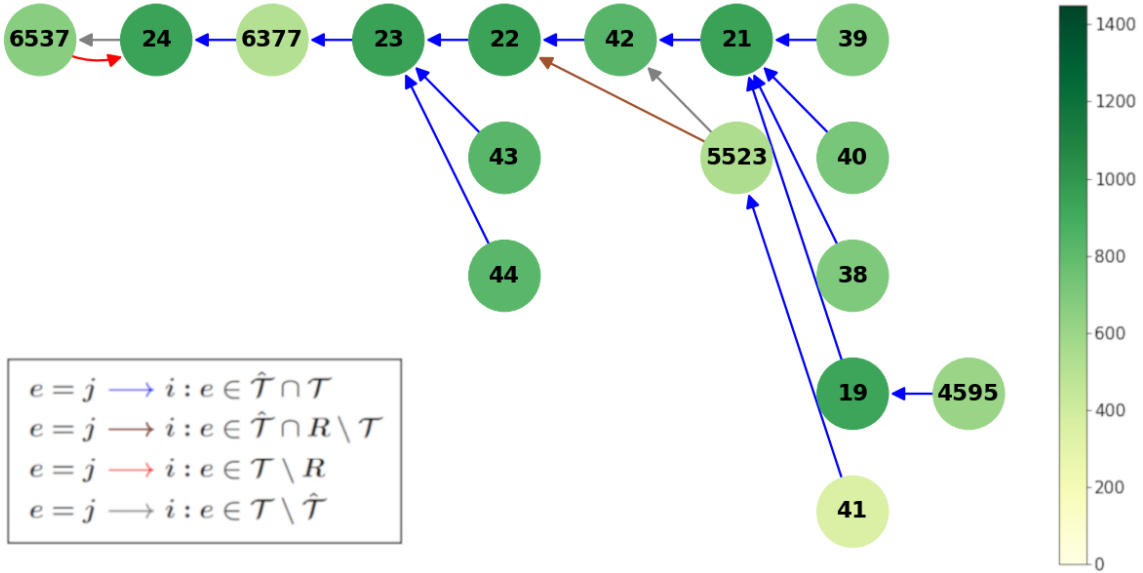
$$\text{nSHD}(\hat{G}, G) := \frac{\text{SHD}(\hat{G}, G)}{|E(\hat{G})| + |E(G)|},$$

where $|E(G)|$ are the number of edges in G . Let $|E(\hat{G}) \setminus E(G)|$ be the number of edges in \hat{G} that are not in G including both, wrong and reversed edges. Moreover, let $|E(\hat{G}) \cap E(G)|$ be the set of estimated edges with correct direction. We then have

$$\begin{aligned} \text{TPR}(\hat{G}, G) &:= \frac{|E(\hat{G}) \cap E(G)|}{|E(G)|}, \\ \text{FDR}(\hat{G}, G) &:= \frac{|E(\hat{G}) \setminus E(G)|}{|E(\hat{G})|}, \end{aligned}$$



(a) Estimated lower Colorado. Node colors represent the amount of available data after declustering.



(b) Estimated lower Colorado where nodes with less than 150 observations have been removed, as these translate to less than 14 observations available to QTree at any fitting iteration. Compared to the full lower Colorado network in part (a), this is a significant improvement.

Fig 8: Estimated (trimmed and untrimmed) lower Colorado. (a): based on all 21 nodes, (b): based on 16 nodes

$$\text{FPR}(\hat{G}, G) := \frac{|E(\hat{G}) \setminus E(G)|}{|V| \times (|V| - 1) - |E(G)|}.$$

Note that for the unnormalized structural Hamming distance, $\text{SHD}(G, \hat{G}) \leq |E(G)| + |E(\hat{G})|$, and this equality is realized when G and \hat{G} have no undirected edges in common, in which case

one needs $|E(G)|$ many deletions and $|E(\hat{G})|$ many additions to transform G to \hat{G} . Therefore, this normalization is designed so that nSHD, like all the other metrics, lies between 0 and 1. We apply these four metrics to both $(\hat{\mathcal{T}}, \mathcal{T})$ and their respective reachability graphs $(\hat{\mathcal{R}}, \mathcal{R})$. With the exception of TPR, the lower the number, the better the performance. The results can be found in Table 4.3.

	Danube		Lower Col.		Middle Col.	Upper Col.
	CQ ¹	QTree	Original	Trimmed		
	Tree estimation $(\hat{\mathcal{T}}, \mathcal{T})$					
nSHD	0.77	0.18	0.45	0.1	0.09	0.13
TPR	0.26	0.8	0.5	0.87	0.9	0.88
FDR	0.8	0.2	0.5	0.13	0.09	0.13
FPR	0.04	0.01	0.02	0.01	0.01	0.02
	Reachability graph estimation $(\hat{\mathcal{R}}, \mathcal{R})$					
nSHD	0.56	0.09	0.15	0.12	0.06	0.02
TPR	0.29	0.87	0.74	0.78	1	0.95
FDR	0.1	0.05	0.02	0.02	0.1	0
FPR	0.01	0.01	0.01	0.01	0.02	0
Total number est. edges	41	30	20	15	11	8
Wrong, stream-connected (brown)	30	4	8	1	0	1
Wrong other edges (red)	3	2	2	1	1	0
Total wrong edges	33	6	10	2	1	1

¹ For comparison: performance based on expected quantile scores as described in [29].

TABLE 4.3

All four metrics for the pairs $(\hat{\mathcal{T}}, \mathcal{T})$ and $(\hat{\mathcal{R}}, \mathcal{R})$ and edge counts. Except for the TPR, smaller values are better. Except for CQ, all rivers have been estimated using QTree with automated parameter selection (cf. Algorithm 2).

Overall, QTree with automated parameter selection has a consistent performance across all data sets, with nSHD and FDR ranging around 10-20%, TPR around 80-90% and FPR close to 0 for the Danube as well as the lower(trimmed), middle and upper Colorado. Comparing the results of QTree with the estimation method based on expected quantile scores and an algorithm using minimum description length that has been advocated in [29], we find a substantial improvement in every considered metric. For the lower(untrimmed) Colorado, QTree still performs well, however, not quite as precise as for the other three. For the reachability graph, the statistics are even better: nSHD, FDR and FPR are below 9% and TPR is over 87% for Danube, lower(trimmed), middle and upper Colorado. For the lower(untrimmed) Colorado, the difference is even larger, as the nSHD decreases to just 15% and the TPR went up to 74%. We therefore conclude that the false edges tend to be from an ancestor to a child, rather than a spurious edge.

5. Performance of the parameter selection method. We want to evaluate the performance of the parameter selection that we have proposed. In theory, if the method works properly, then we should choose q such that nSHD, TPR, FDR and FPR are optimal for both pairs $(\hat{\mathcal{T}}, \mathcal{T})$ and $(\hat{\mathcal{R}}, \mathcal{R})$.

In Figure 9, we plotted the nSHD, TPR, FDR and FPR for the Danube. The blue curve shows the result for $(\hat{\mathcal{T}}, \mathcal{T})$ and the green curve for $(\hat{\mathcal{R}}, \mathcal{R})$. For each q we have $\mathcal{T}_q := \{T^1, \dots, T^{1000}\}$ of estimated trees based on 1000 subsamples that we have chosen randomly. We then addi-

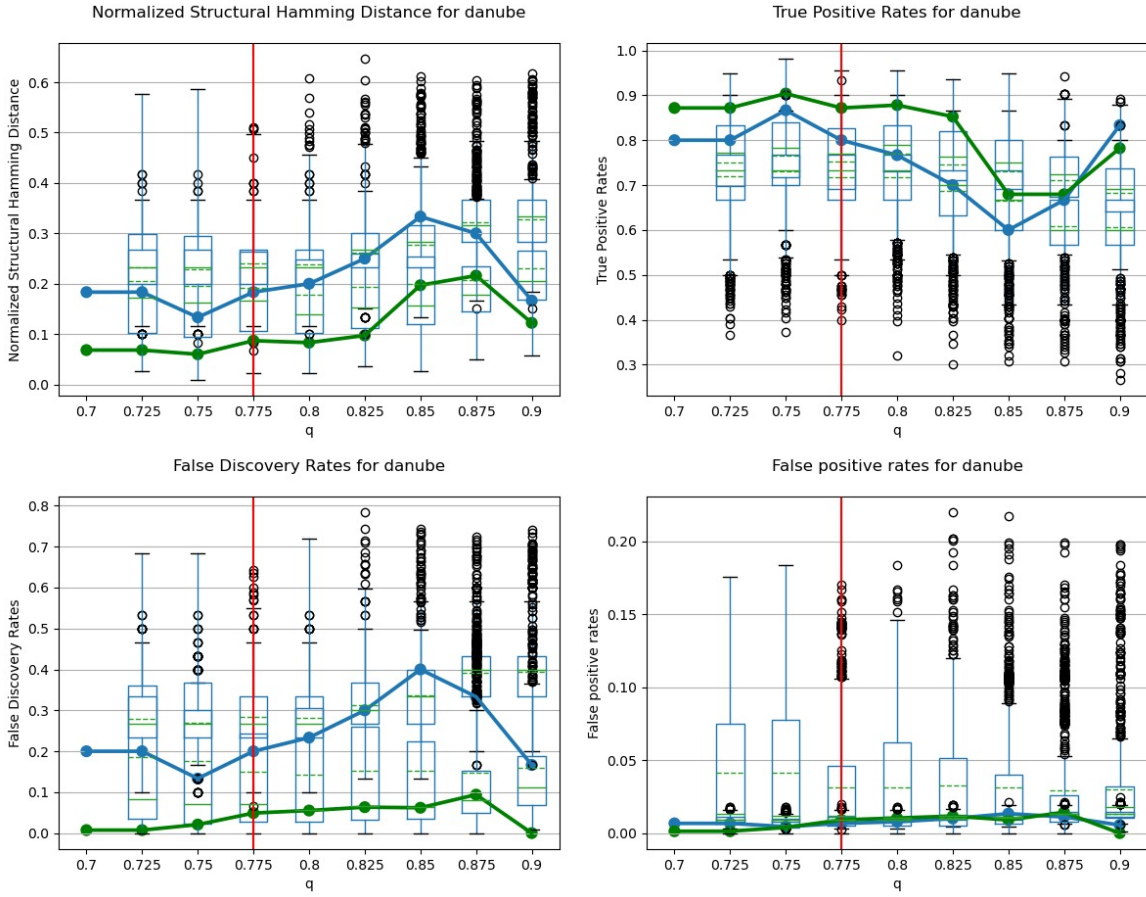


Fig 9: Metrics nSHD, TPR, FDR and FPR for the Danube and varying parameters q : boxplots for the metrics of $m = 1000$ trees of \mathcal{T}_q , blue dots on a line represent the respective metrics for $(\hat{\mathcal{T}}, \mathcal{T})$; green dots on a line represent the respective metrics for the pair (\hat{R}, R) . The vertical red line indicates the variation-minimizing q chosen by Algorithm 2.

tionally display boxplots of the respective metrics of \mathcal{T}_q with its centroid $\mathbb{E}(\mathcal{T}_q)$ as in (2.9). The vertical red line indicates the variation-minimizing q chosen by Algorithm 2.

For the Danube, all three metrics (nSHD, FDR and FPR) are close to their minimum for the chosen $q = 0.775$ while the TPR is close to its maximum. Note that $q = 0.75$ would have led to an even better estimation (cf. Figure 12). However, we can see through the underlying boxplot that for $q = 0.75$, the subsamples have more varying performances relative to its centroid compared to $q = 0.775$, indicating that the parameter selection procedure behaved as expected. The Hamming distance between the centroids of $q = 0.775$ and $q = 0.75$ is also small, consisting of exactly 2 edges concerning the nodes 2, 14 and 15. Thus, this indicates that the output of Algorithm 2 is quite stable, with small changes in q leading to small, local changes in the estimated tree.

Figure 10 depicts the parameter selection for the upper Colorado. For this data set, QTree Algorithm 2 returns $q = 0.825$. Again, the method works extremely well. However, in this case the choice of the parameter q for the given data set is again not optimal, as $q = 0.9$ would have given us perfect recovery of the upper Colorado.

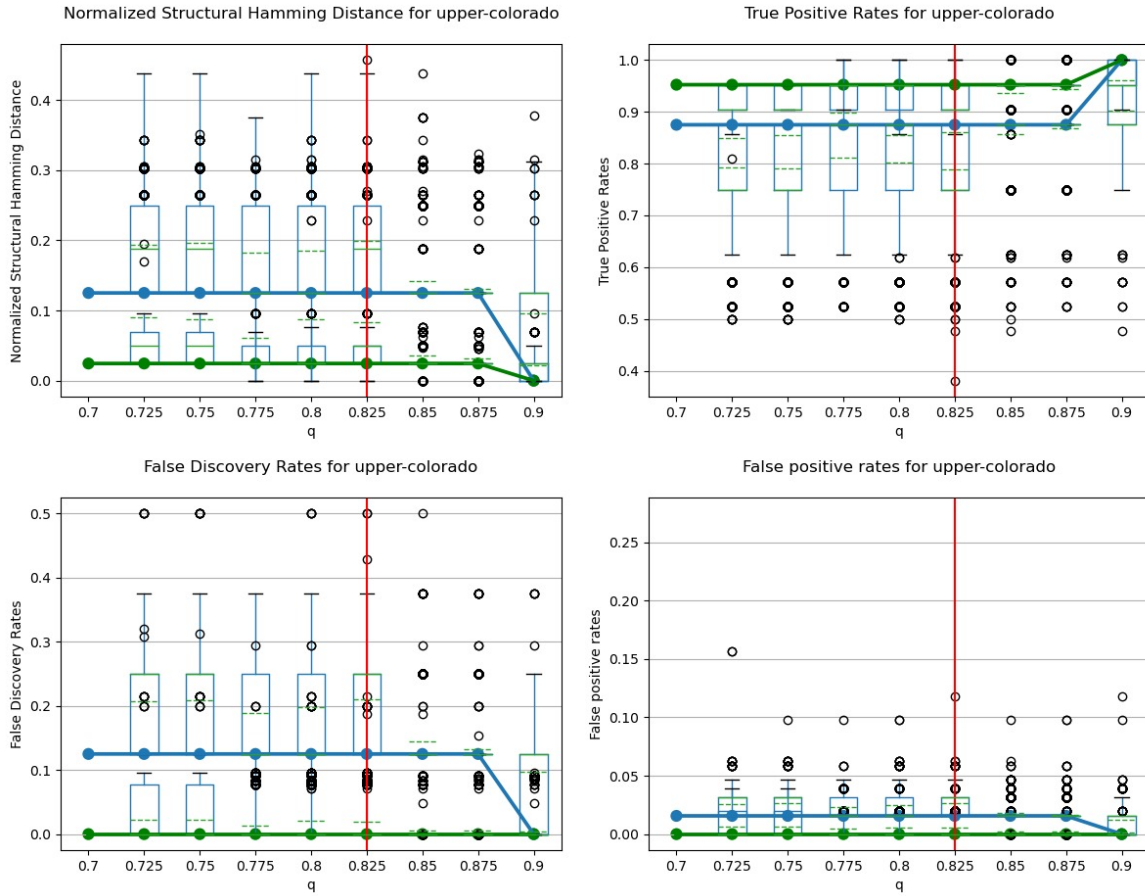


Fig 10: Metrics nSHD, TPR, FDR and FPR for the upper Colorado and varying parameters q : boxplots for the metrics of $m = 1000$ trees of \mathbb{T}_q , blue dots on a line represent the respective metrics for $(\hat{\mathcal{T}}, \mathcal{T})$; green dots on a line represent the respective metrics for the pair (\hat{R}, R) . The vertical red line indicates the variation-minimizing q chosen by Algorithm 2.

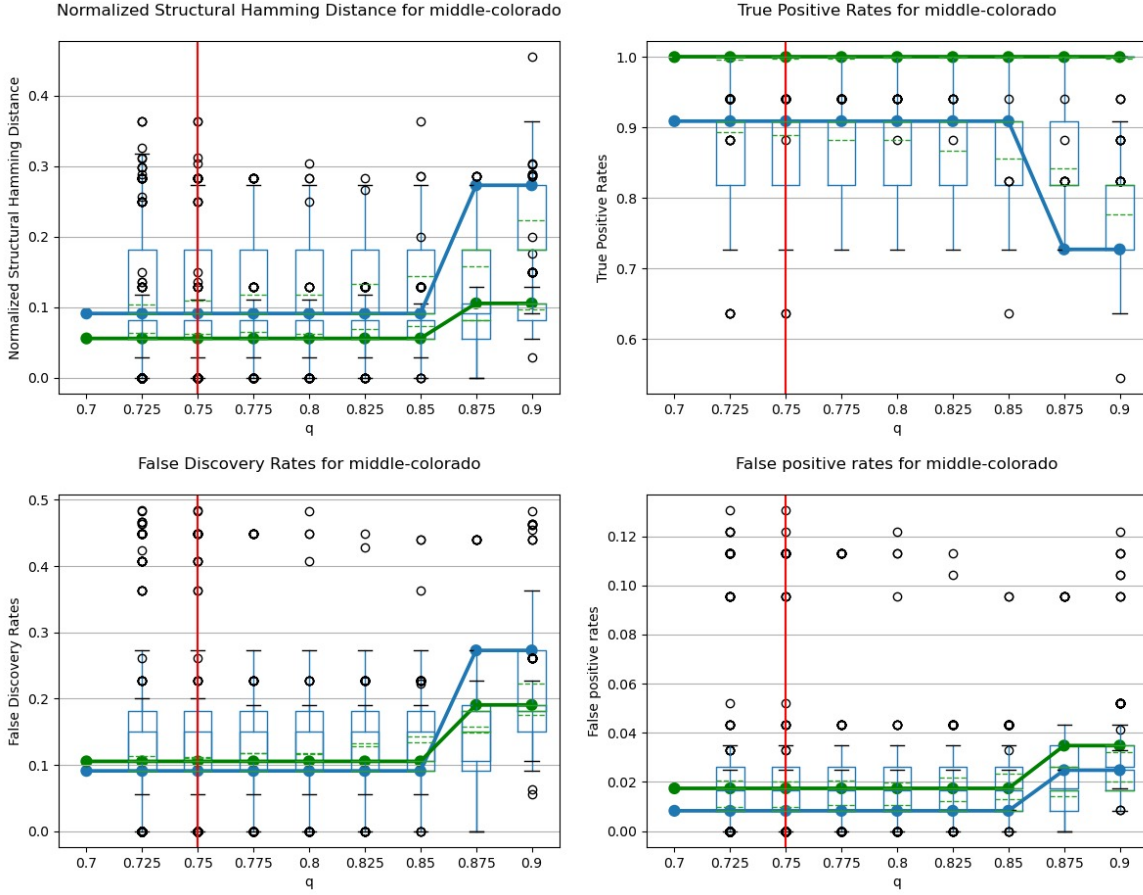


Fig 11: Metrics nSHD, TPR, FDR and FPR for the middle Colorado and varying parameters q : boxplots for the metrics of $m = 1000$ trees of \mathcal{T}_q , blue dots on a line represent the respective metrics for $(\hat{\mathcal{T}}, \mathcal{T})$; green dots on a line represent the respective metrics for the pair (\hat{R}, R) . The vertical red line indicates the variation-minimizing q chosen by Algorithm 2.

For the middle Colorado in Figure 11, QTree Algorithm 2 returns $q = 0.75$, which is the best choices for q . Finally, the result of the parameter selection for the lower Colorado as shown in Figure 13 is most interesting. For the full data set there seems to be a trade-off, as for the pair $(\hat{\mathcal{T}}, \mathcal{T})$ the optimal choice of q is around $q = 0.725$ and, hence, very different from the optimal choice for (\hat{R}, R) at around $q = 0.85$. However, the improvement for the reachability graph from $q = 0.725$ to $q = 0.85$ is much larger than the worsening of the tree. Therefore, the parameter selection again works very well. Moreover, for the trimmed lower Colorado, where we neglected all nodes with less than 150 observations, the choice of the parameter selection is again among the best. We conclude that QTree is robust on the choice of q as for all 5 data sets we can achieve good results for q ranging between 0.7 and 0.85. However, the choice of the parameter selection sometimes does not output the best result. For example, for the Danube the parameter $q = 0.75$ would have let to a much better result (cf. Figure 12). Also for the upper Colorado, $q = 0.9$ would have been given a perfect recovery of the underlying network, see Figure 10.

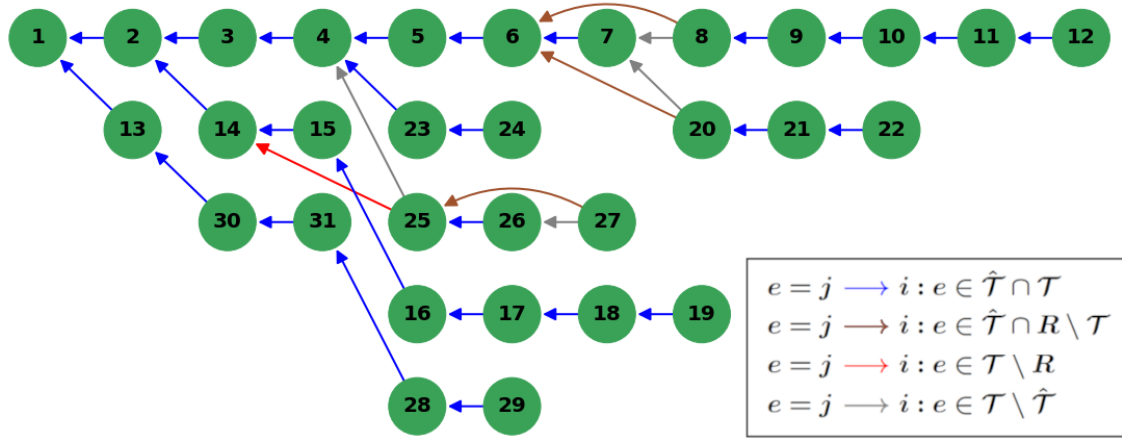


Fig 12: Estimated Danube network for $q = 0.75$. Blue edges are correct edges, brown edges are wrong in graph but correct in reachability, red edges are wrong in graph and reachability, gray edges are missing edges.

6. Summary. In this paper, we have solved the hidden river problem. While max-linear Bayesian networks have served as motivation, the algorithm successfully detects the (almost) correct tree, confirming that our learning algorithm is very robust.

For each potential edge $j \rightarrow i$, we assign a score d_{ij} which measures data dispersion around a low quantile \underline{r} , which measures how concentrated the data $x_j - x_i$ is near its minimum. Here, we only use “high quality” observations from the data in the upper tail, more precisely data larger than a high quantile q .

Algorithm 1 estimates for given q and \underline{r} the score matrix D , calculates the minimal root-directed spanning arborescence \hat{T} of D using the Edmond-Chu-Liu algorithm. Algorithm 2 provides an automated parameter selection for q and \underline{r} by a bootstrap-like procedure. While the parameter selection reliably gives good tuning parameters, we have seen that the choice is sometimes not optimal. Future research directions include choosing and proving the optimality of alternative variability metrics for Algorithm 2, or having the algorithm output a distribution over possible root-directed trees instead of a single best tree.

We test our algorithm for rivers and their tributaries in the Danube River Basin and for three sections of the Lower Colorado Basin with great success, outperforming existing methods clearly. We also present certain metrics to assess the quality of graph recovery by performance metrics and the performance of the variable selection confirming again the success of our new method. The accompanying paper [8] provides a consistency prove of the estimated tree.

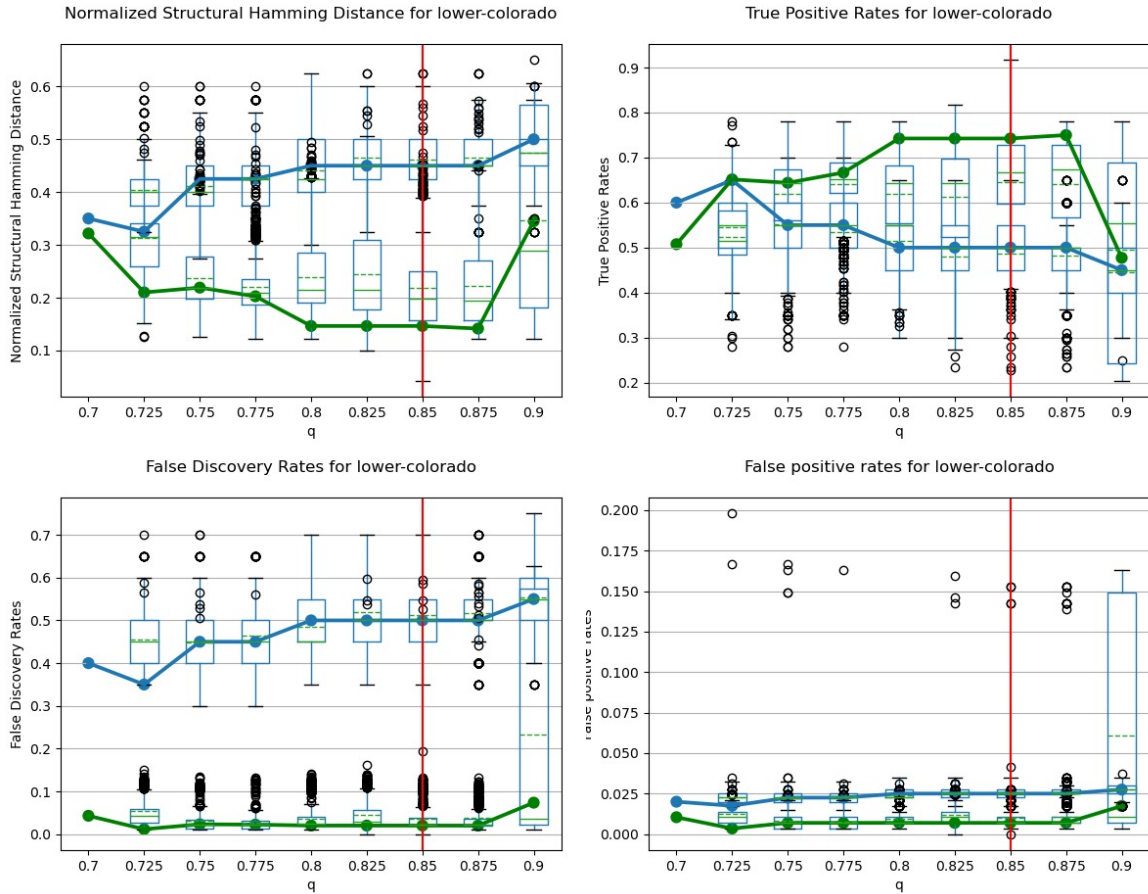


Fig 13: Metrics nSHD, TPR, FDR and FPR for the lower Colorado and varying parameters q : boxplots for the metrics of $m = 1000$ trees of \mathcal{T}_q , blue dots on a line represent the respective metrics for $(\hat{\mathcal{T}}, \mathcal{T})$; green dots on a line represent the respective metrics for the pair (\hat{R}, R) . The vertical red line indicates the variation-minimizing q chosen by Algorithm 2.

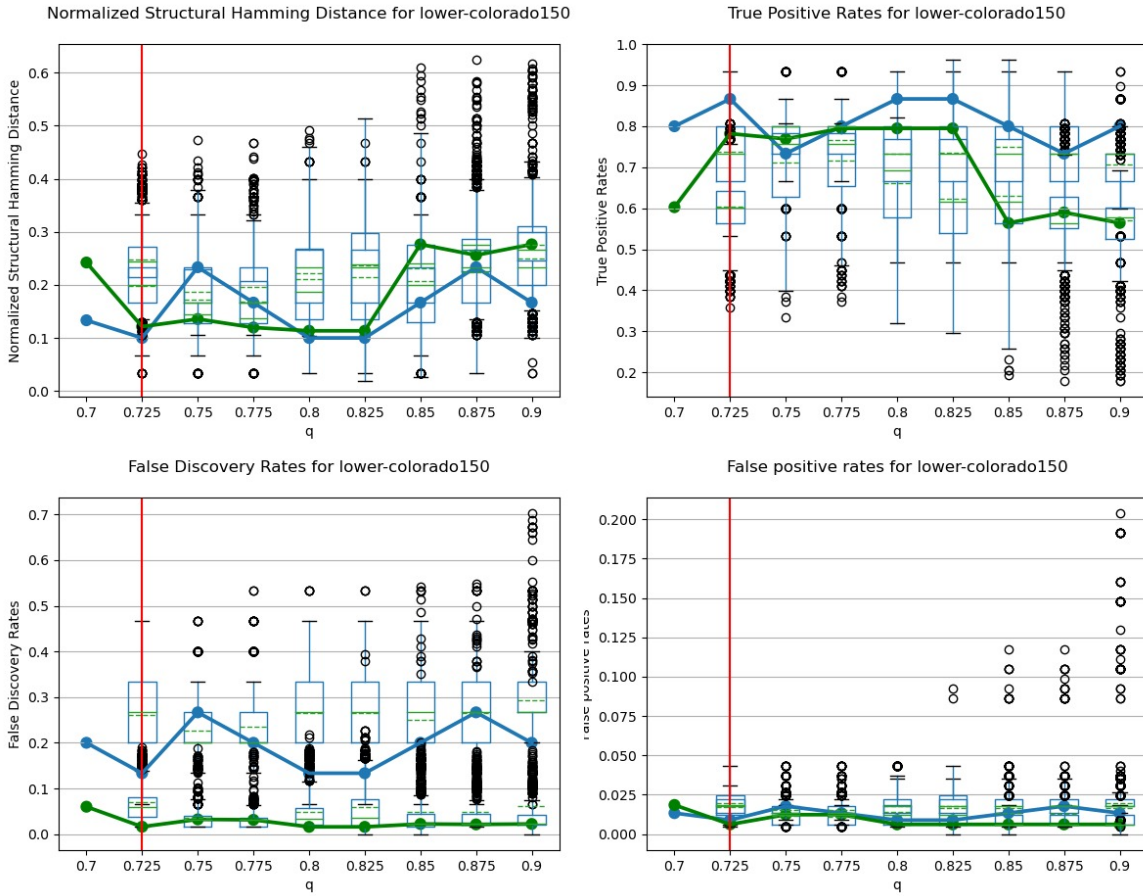


Fig 14: Metrics nSHD, TPR, FDR and FPR for the trimmed lower Colorado and varying parameters q : boxplots for the metrics of $m = 1000$ trees of T_q , blue dots on a line represent the respective metrics for (\hat{T}, \mathcal{T}) ; green dots on a line represent the respective metrics for the pair (\hat{R}, R) . The vertical red line indicates the variation-minimizing q chosen by Algorithm 2.

REFERENCES

- [1] C. Améndola, C. Klüppelberg, S. Lauritzen, and N. M. Tran. Conditional independence in max-linear Bayesian networks. *Ann. Appl. Prob.*, 2019. To appear, arXiv:2002.09233v2.
- [2] M. P. Anderson, W. W. Woessner, and R. J. Hunt. *Applied groundwater modeling: simulation of flow and advective transport*. Academic press, 2015.
- [3] P. Asadi, A. C. Davison, and S. Engelke. Extremes on river networks. *Annals of Applied Statistics*, 9(4):2023–2050, 2015.
- [4] M. Bartos, B. Wong, and B. Kerkez. Open storm: a complete framework for sensing and control of urban watersheds. *Environmental Science: Water Research & Technology*, 4(3):346–358, 2018.
- [5] A. Boneh and M. Hofri. The coupon-collector problem revisited—a survey of engineering problems and computational methods. *Stochastic Models*, 13(1):39–66, 1997.
- [6] S. Boneh and V. G. Papanicolaou. General asymptotic estimates for the coupon collector problem. *Journal of Computational and Applied Mathematics*, 67(2):277–289, 1996.
- [7] J. Buck and C. Klüppelberg. Recursive max-linear models with propagating noise. *arXiv preprint arXiv:2003.00362*, 2020.
- [8] J. Buck, C. Klüppelberg, and N. Tran. Consistency of QTree under observational noise. *In preparation*, 2021.
- [9] D. M. Chickering. Learning Bayesian networks is np-complete. In *Learning from data*, pages 121–130. Springer, 1996.
- [10] Y. Chu and T. Liu. On the shortest arborescence of a directed graph. *Science Sinica*, (14):1396–400, 1965.
- [11] S. Engelke and A. Hitz. Graphical models for extremes. *JRSS B*, 82:871–932, 2020.
- [12] H. N. Gabow, Z. Galil, T. Spencer, and R. E. Tarjan. Efficient algorithms for finding minimum spanning trees in undirected and directed graphs. *Combinatorica*, 6(2):109–122, 1986.
- [13] N. Gissibl. *Graphical Modeling of Extremes: Max-linear models on directed acyclic graphs*. Ph.D. thesis, Technical University of Munich, 2018.
- [14] N. Gissibl and C. Klüppelberg. Max-linear models on directed acyclic graphs. *Bernoulli*, 24(4A):2693–2720, 2018.
- [15] N. Gissibl, C. Klüppelberg, and M. Otto. Tail dependence of recursive max-linear models with regularly varying noise variables. *Econometrics and Statistics*, 6:149 – 167, 2018.
- [16] N. Gissibl, C. Klüppelberg, and S. L. Lauritzen. Identifiability and estimation of recursive max-linear models. *Scandinavian Journal of Statistics*, 2020. . arXiv:1901.03556.
- [17] N. Gnecco, N. Meinshausen, J. Peters, and S. Engelke. Causal discovery in heavy-tailed models. *arXiv preprint arXiv:1908.05097*, 2019.
- [18] A. Hannart and P. Naveau. Probability of causation of climate changes. *Journal of Climate Change*, 31(14):5507–5524, 2018.
- [19] A. Hannart, J. Pearl, F. Otto, P. Naveau, and M. Ghil. Causal counterfactual theory for the attribution of weather and climate-related events. *Bulletin of the American Meteorological Society*, 97:99–110, 2016.
- [20] A. Kiriliouk and P. Naveau. Climate extreme event attribution using multivariate peaks-over-thresholds modeling and counterfactual theory. *Ann. Appl. Statistics*, 14(3):1342–1358, 2020.
- [21] C. Klüppelberg and M. Krali. Estimating an extreme Bayesian network via scalings. *Journal of Multivariate Analysis*, 2021. <https://doi.org/10.1016/j.jmva.2020.104672>.
- [22] C. Klüppelberg and S. Lauritzen. Bayesian networks for max-linear models. In F. Biagini, G. Kauermann, and T. Meyer-Brandis, editors, *Network Science - An Aerial View from Different Perspectives*. Springer, 2020.
- [23] C. Leigh, O. Alsibai, R. J. Hyndman, S. Kandanaarachchi, O. C. King, J. M. McGree, J. S. Catherine Neelamraju, P. D. Talagala, R. D. Turner, K. Mengersen, and E. E. Peterson. A framework for automated anomaly detection in high frequency water-quality data from in situ sensors. *Science of The Total Environment*, 664(5):885–898, 2019.
- [24] Lower Colorado River Authority (LCRA). Private correspondence, 2020.
- [25] Lower Colorado River Authority (LCRA). Highland lakes and dams, Accessed August 2020. <https://www.lcra.org/water/dams-and-lakes>.

- [26] Lower Colorado River Authority (LCRA). Lower Colorado River Authority dataset, Accessed August 2020.
- [27] F. Mao, K. Khamis, S. Krause, J. Clark, and D. M. Hannah. Low-cost environmental sensor networks: recent advances and future directions. *Frontiers in Earth Science*, 7:221, 2019.
- [28] S. J. McGrane. Impacts of urbanisation on hydrological and water quality dynamics, and urban water management: a review. *Hydrological Sciences Journal*, 61(13):2295–2311, 2016.
- [29] L. Mhalla, V. Chavez-Demoulin, and D. J. Dupuis. Causal mechanism of extreme river discharges in the upper danube basin network. *Journal of the Royal Statistical Society: Series C (Applied Statistics)*, 69(4):741–764, 2020.
- [30] D. R. Musser. Introspective sorting and selection algorithms. *Software: Practice and Experience*, 27(8):983–993, 1997.
- [31] J. Rodriguez-Perez, C. Leigh, B. Lique, C. Kermorvant, E. Peterson, D. Sous, and K. Mengersen. Detecting technical anomalies in high-frequency water-quality data using artificial neural networks. *Environmental Science & Technology*, 54(21):13719–13730, 2020.
- [32] N. M. Tran. QTree Python Implementation. <https://github.com/princengoc/mtree>, 2021.
- [33] J. M. Ver Hoef and E. Peterson. A moving average approach for spatial statistical models of stream networks. *Journal of the American Statistical Association*, 105(489):6–18, 2010.
- [34] J. M. Ver Hoef, E. Peterson, and D. Theobald. Spatial statistical models that use flow and stream distance. *Environmental and Ecological Statistics*, 13(4):449–464, 2006.
- [35] M. J. Wainwright and M. I. Jordan. *Graphical models, exponential families, and variational inference*. Now Publishers Inc, 2008.
- [36] L. Wolf, C. Zwiener, and M. Zemann. Tracking artificial sweeteners and pharmaceuticals introduced into urban groundwater by leaking sewer networks. *Science of The Total Environment*, 430:8–19, 2012. .
- [37] X. Zheng, B. Aragam, P. K. Ravikumar, and E. P. Xing. Dags with no tears: Continuous optimization for structure learning. In *Advances in Neural Information Processing Systems*, volume 31, pages 9472–9483. Curran Associates, Inc., 2018.

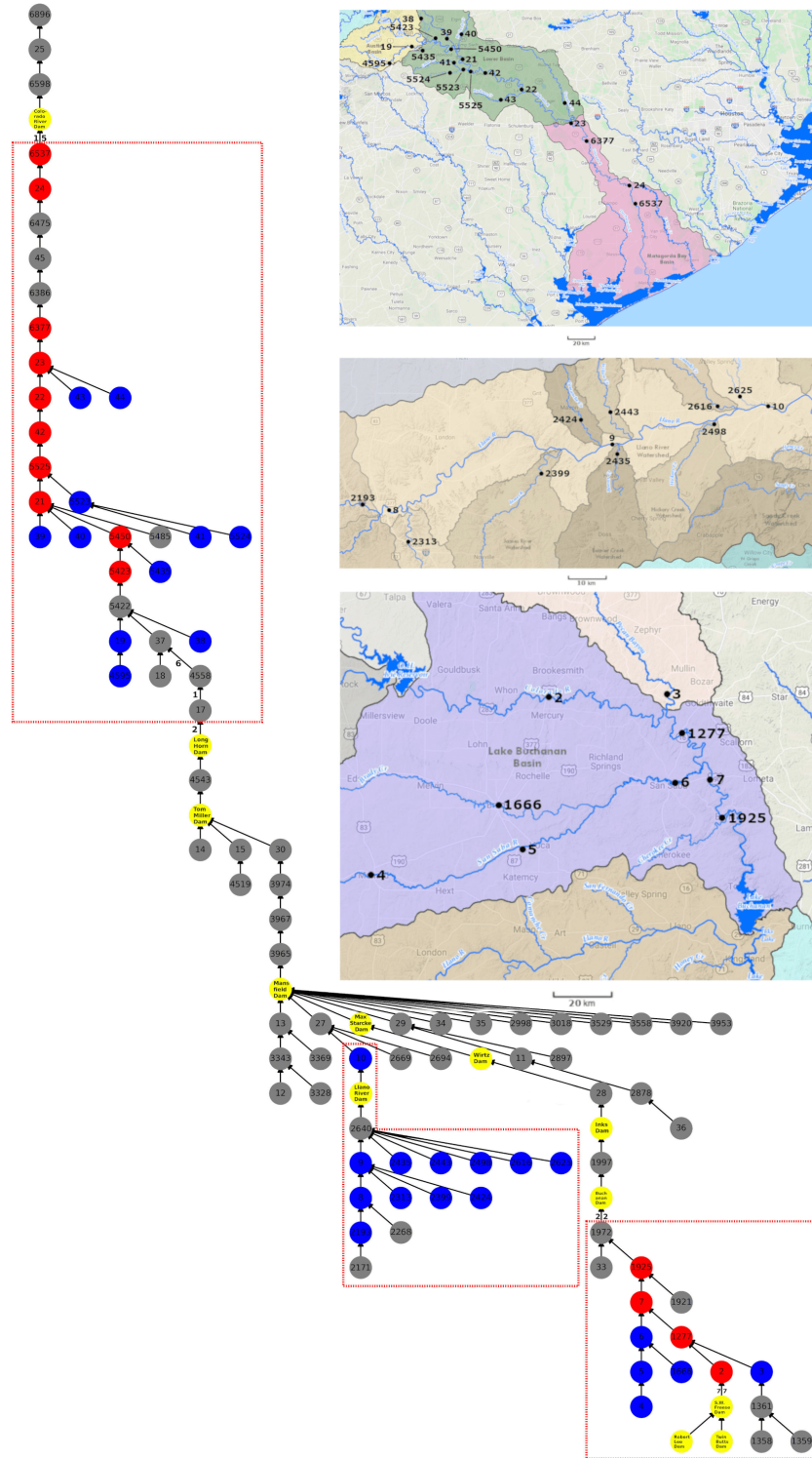


Fig 15: Lower Colorado River: sections framed in red represent the lower, middle and upper sections, gray nodes are not being considered. Pictures on the right show geographic maps of the lower, middle and upper Colorado, respectively.